Coupled S waves in inhomogeneous weakly anisotropic media using first-order ray tracing

Véronique Farra [1] and Ivan Pšenčík [2]

[1] *Institut de Physique du Globe de Paris*, 4 *Place Jussieu*, 75252 *Paris Cedex* 05, *France. E-mail: farra@ipgp.jussieu.fr*
[2] *Institute of Geophysics, Acad. Sci. of Czech Republic, Boční II*, 141 31 *Praha* 4, *Czech Republic. E-mail: ip@ig.cas.cz*

SUMMARY

We present a generalization of the recently proposed approximate procedure for computing coupled S waves in inhomogeneous weakly anisotropic media. The new procedure can be used to compute S waves propagating in smooth inhomogeneous isotropic or anisotropic media. In isotropic media, it reduces to standard S-wave ray tracing. In anisotropic media, it can be used to study coupled as well as decoupled S waves. As the previous procedure, the new one is also based on the approximately computed common S-wave ray. First-order ray and dynamic ray tracing, originally developed for computations of P-wave fields, is used to compute common S-wave rays and the dynamic ray tracing along it. The principal difference between the previous and new procedure consists in a substantial increase of accuracy of the coupling equations, which are solved along the common ray to evaluate S-wave amplitudes. The new coupling equations provide, first of all, more accurate traveltimes.

The new procedure has all the advantages of the previous procedure. Among the basic advantages is that it can describe the coupling of S waves. The procedure eliminates problems with ray tracing in the vicinity of singularities; the common S-wave ray tracing is as stable as P-wave ray tracing. Due to the use of perturbation formulae, the ray tracing, dynamic ray tracing and coupling equations are much simpler and more transparent than in the exact case. There is no need to construct a reference medium as, for example, in the quasi-isotropic approach. As a byproduct of both coupling procedures, we get formulae for approximate evaluation of traveltimes of separate S waves. These formulae can find applications in migration and traveltime tomography.

The accuracy of the previous and new coupling procedures is studied on several models of varying strength of anisotropy. First, we investigate the accuracy of perturbation formulae in homogeneous models, in which coupling does not exist. Then we study both coupling and perturbation effects in inhomogeneous models. We compare the results

Seismic Waves in Complex 3-D Structures, Report 19, Department of Geophysics, Faculty of Mathematics and Physics, Charles University, Praha 2009, pp.63-91

obtained with the coupling procedures with the results of the quasi-isotropic approach and standard ray theory.

Keywords: Body waves; Seismic anisotropy; Wave propagation.

1 INTRODUCTION

S waves propagating in inhomogeneous, weakly anisotropic media are usually coupled. Coupling can be described, for example, by the "connection" formulae (Thomson et al., 1992) or by the coupling ray theory (Coates & Chapman, 1990; Bulant & Klimeš, 2002). There are various versions of the coupling ray theory, which differ in the choice of the trajectory - common S-wave ray - along which coupling effects are evaluated, or by various approximations of the coupling equations. For an extensive review of such approximations, see Klimeš & Bulant (2004).

One of the approximations of the coupling ray theory is the quasi-isotropic approach. It was proposed by Kravtsov (1968), see also Kravtsov & Orlov (1990). Later it was applied by Pšenčík (1998) to elastic media, see also Pšenčík & Dellinger (2001). In the quasi-isotropic approach, the common S-wave ray is traced in a reference isotropic medium approximating the studied anisotropic medium. This reduces the accuracy of the corresponding computations. In order to increase their accuracy, Bakker (2002) proposed the use of the common S-wave ray, which is traced in the studied anisotropic medium, see also Klimeš (2006). Farra & Pšenčík (2008), hereinafter referred to as Paper I, used Bakker's (2002) approach and combined it with the first-order ray tracing (FORT) and first-order dynamic ray tracing (FODRT) concept, which they used before for computating P waves in inhomogeneous weakly anisotropic media (Pšenčík & Farra, 2005, 2007).

As in the papers on FORT and FODRT for P waves, the computation of common S-wave rays and dynamic ray tracing along them in Paper I is also based on the perturbation theory, in which deviations of anisotropy from isotropy are considered to be small. The trajectory of the common S-wave ray corresponds to the Hamiltonian obtained from the average of the first-order eigenvalues of the Christoffel matrix, corresponding to the two S waves propagating in anisotropic media. The common S-wave ray is computed in the studied medium and, therefore, it does not require the specification of a reference medium as in the quasi-isotropic approach. The reference medium in Paper I is only necessary for computating the second-order common S-wave traveltime corrections. The great advantage of such common S-wave rays is that their computation does not collapse in the vicinity of S-wave singularities as is typical for standard S-wave ray tracing in anisotropic media, see, e.g., Vavryčuk (2003). The use of the common S-wave ray computed in the studied anisotropic medium is advantageous even in homogeneous media, where all common rays between the source and the receiver coincide. The quantities calculated along the common ray (for example, the slowness vector) in the studied anisotropic medium approximate the actual quantities better.

The approximate coupling equations are derived in Paper I under the assumption that

the deviations of anisotropy from isotropy are, simply speaking, of the order $O(\omega^{-1})$, where ω is the circular frequency. The coupling equations consist of two coupled, frequency-dependent, linear, ordinary, differential equations for the S-wave amplitude coefficients and are solved along common S-wave rays.

In this paper, we propose a simple generalization of the coupling equations proposed in Paper I, which considerably increases their accuracy. The generalization consists in substituting two mutually perpendicular unit vectors, which define the zero-order polarization plane of the common S wave in Paper I, by vectors, which define the polarization plane more accurately. The expressions for the new vectors are very simple. Their use, however, leads not only to an improved description of polarization, but, most importantly, to a considerable increase of the accuracy of traveltimes. No reference medium is required.

There is a considerable difference between the formulation of the coupling ray theory studied by Klimeš & Bulant (2004) or Bulant & Klimeš (2008) and the approach presented in this paper. In our approach, the common ray computation, dynamic ray tracing and coupling equations along it are approximate. The traveltime corrections are incorporated in the coupling equations. There is no need for additional numerical quadratures along the common S-wave ray. Despite the differences in formulation, general conclusions are very similar. The proposed scheme can describe S-wave propagation in smooth inhomogeneous isotropic media (it reduces there to the standard ray tracing for isotropic media), and it describes, with sufficient accuracy, the coupling of S waves in smooth inhomogeneous, weakly anisotropic media and, as the presented synthetic tests illustrate, can even describe properly well separated S waves.

An interesting and useful byproduct of the coupling equations are approximate formulae for computing traveltimes and polarizations of separate S waves propagating in inhomogeneous anisotropic media. The formulae are simple and transparent. We can distinguish in them the terms responsible for S1- and S2-wave traveltime separation and terms responsible for corrections of the traveltime along the common S-wave ray.

In Sec.2, we review the main results of Paper I, which include FORT and FODRT for the common S-wave ray, and coupling equations. In Sec.3, we derive generalized coupling equations. These equations represent one of the basic contributions of this paper. Sec.4 is devoted to the illustration of the performance of both types of approximate coupling equations on several models of varying strength of anisotropy. On homogeneous models, in which coupling does not exist, we study the accuracy of the proposed formulae. On inhomogeneous models, we compare the results obtained with the coupling equations presented in Paper I and here with the results of the standard ray theory or of the quasi-isotropic approach. Advantages and limitations and future plans are briefly discussed in Sec.5. Finally, in Appendix A, we study the behaviour of coupling equations, derived in Paper I and herein, in special cases. We describe how equations reduce in isotropic media or in media with stronger anisotropy or weaker inhomogeneity or for higher frequencies. Approximate formulae for computing separate S-wave traveltimes are also given there.

The lower-case indices $i, j, k, l, ...$ take the values of 1,2,3, the upper-case indices $I, J, K, L, ...$ take the values of 1,2. The Einstein summation convention over repeated indices is used. The upper index $[\mathcal{M}]$ is used to denote quantities related to the S-wave common ray.

2 BASIC EQUATIONS

In the frequency domain, the zero-order ray approximation of the displacement vector $\mathbf{u}$ of an arbitrary wave propagating in an inhomogeneous anisotropic medium can be expressed as:

$$\mathbf{u}(x_m, \omega) = \mathbf{U}(x_m)\exp[\mathrm{i}\omega\tau(x_m)]. \tag{1}$$

Here i is the imaginary unit, ω is the circular frequency, $\tau(x_m)$ is the eikonal, which also serves as the traveltime, and $\mathbf{U}(x_m)$ is the zero-order vectorial amplitude coefficient. Expression (1) is a good approximation of the displacement vector if the variations of the model and wave parameters within a wavelength are small, in other words if characteristic length L (the distance, on which the parameters change by an amount comparable with their size) is large. This condition can be expressed as the requirement that parameter $\epsilon_1 \sim c/(\omega L)$ is small (Pšenčík, 1998). This requirement is often simplified to $\epsilon_1 \sim \omega^{-1}$, see, e.g., Paper I. Here we use the more general former definition of ϵ_1, i.e., $\epsilon_1 \sim c/(\omega L)$.

As in Paper I, we concentrate on the coupled S waves computed along a common S-wave ray and assume that in an inhomogeneous weakly anisotropic medium the vectorial amplitude coefficient $\mathbf{U}(x_m) = \mathbf{U}[x_m(\tau)]$ has the form:

$$\mathbf{U}(\tau) = \mathcal{A}(\tau)\mathbf{e}^{[1]}(\tau) + \mathcal{B}(\tau)\mathbf{e}^{[2]}(\tau). \tag{2}$$

In (2), $\mathcal{A}$ and $\mathcal{B}$ are S-wave amplitude coefficients and vectors $\mathbf{e}^{[1]}$ and $\mathbf{e}^{[2]}$ are mutually perpendicular unit vectors, to which the amplitude coefficients are related. Parameter τ is the traveltime. All the mentioned quantities are computed along the S-wave common ray, obtained by solving the first-order ray-tracing (FORT) equations:

$$\frac{dx_i}{d\tau} = \frac{1}{2}\frac{\partial G^{[\mathcal{M}]}(x_m, p_m)}{\partial p_i}, \qquad \frac{dp_i}{d\tau} = -\frac{1}{2}\frac{\partial G^{[\mathcal{M}]}(x_m, p_m)}{\partial x_i}. \tag{3}$$

Here x_i and p_i are the Cartesian coordinates of the S-wave common first-order ray and the components of the corresponding first-order slowness vectors, respectively. Parameter $\tau = \tau^{[\mathcal{M}]}(x_m)$ is the first-order traveltime. Symbol $G^{[\mathcal{M}]}$ denotes the first-order S-wave mean eigenvalue

$$G^{[\mathcal{M}]}(x_m, p_m) = \tfrac{1}{2}(G^{[1]} + G^{[2]}) = \tfrac{1}{2}(B_{11} + B_{22}) = \tfrac{1}{2}\Gamma_{ik}(e_i^{[1]}e_k^{[1]} + e_i^{[2]}e_k^{[2]}). \tag{4}$$

In (4), $G^{[1]}$ and $G^{[2]}$ are the first-order approximations of two smaller eigenvalues of the generalized Christoffel matrix $\mathbf{\Gamma}$ (we call it generalized because it contains components of slowness vector $\mathbf{p}$ instead of the unit vector in the direction of $\mathbf{p}$ used in the standard Christoffel matrix):

$$\Gamma_{ik}(x_m, p_m) = a_{ijkl}(x_m)p_j p_l \ . \tag{5}$$

Symbols a_{ijkl} denote density-normalized elastic moduli,

$$a_{ijkl} = c_{ijkl}/\rho \ , \tag{6}$$

c_{ijkl} being elements of the fourth-order tensor of elastic moduli and ρ the density. The first-order S-wave eigenvalues $G^{[1]}$ and $G^{[2]}$ can also be expressed in terms of elements B_{11}, B_{12} and B_{22} of the symmetric matrix $\mathbf{B}(x_m, p_m)$:

$$B_{jl}(x_m, p_m) = \Gamma_{ik}(x_m, p_m)e_i^{[j]}e_k^{[l]}. \tag{7}$$

Symbols $e_i^{[j]}$ in (4) and (7) denote the components of unit vectors $\mathbf{e}^{[j]}$. Vectors $\mathbf{e}^{[1]}$ and $\mathbf{e}^{[2]}$, see (2), are perpendicular to the third vector $\mathbf{e}^{[3]}$ chosen so that $\mathbf{e}^{[3]} = \mathbf{n}$. Here $\mathbf{n}$ is a unit vector specifying the direction of the first-order slowness vector $\mathbf{p}$. Vectors $\mathbf{e}^{[K]}$ can be chosen arbitrarily in the plane perpendicular to $\mathbf{n}$. Vector $\mathbf{e}^{[3]}$ can be determined from the second set of FORT equations (3). Along the common S-wave ray, vectors $\mathbf{e}^{[K]}$ can be computed as the vectorial base of the *wavefront orthonormal coordinate system*, see, e.g., Červený (2001):

$$\frac{de_i^{[K]}}{d\tau} = -(c^{[\mathcal{M}]})^2 (e_k^{[K]} \frac{dp_k}{d\tau}) p_i. \tag{8}$$

Here, $c^{[\mathcal{M}]} = c^{[\mathcal{M}]}(x_m, n_m)$ is the first-order S-wave common phase velocity corresponding to $G^{[\mathcal{M}]}$, $(c^{[\mathcal{M}]})^2 = G^{[\mathcal{M}]}(x_m, n_m)$.

At each point along the ray, the first-order slowness vectors determined from equations (3) satisfy the first-order eikonal equation:

$$G^{[\mathcal{M}]}(x_m, p_m) = [c^{[\mathcal{M}]}(x_m, n_m)]^{-2} G^{[\mathcal{M}]}(x_m, n_m) = 1. \tag{9}$$

Note that an explicit expression for $G^{[\mathcal{M}]}(x_m, p_m)$ in terms of the weak-anisotropy (WA) parameters is given in Paper I.

The point-source initial conditions for the ray-tracing equations (3) for $\tau = \tau_0$ read:

$$x_i(\tau_0) = x_i^0, \qquad p_i(\tau_0) = p_i^0. \tag{10}$$

Here, x_i^0 are the coordinates of source point $\mathbf{x}^0$, and $p_i^0 = n_i^0 / c_0^{[\mathcal{M}]}$ are the components of the first-order slowness vector $\mathbf{p}^0$ at the source. Symbol $c_0^{[\mathcal{M}]}$ denotes the first-order approximation of the S-wave common phase velocity in direction $\mathbf{n}^0$ at source point $\mathbf{x}^0$. Velocity $c_0^{[\mathcal{M}]}$ is given by the square root of $G^{[\mathcal{M}]}(x_m^0, n_m^0)$, see eq. (9). Vector $\mathbf{n^0}$ can be specified by two ray parameters, $\gamma^{(J)}$, chosen as two take-off angles, ϕ_0 and δ_0, so that

$$n_1^0 = \cos\phi_0 \cos\delta_0, \quad n_2^0 = \sin\phi_0 \cos\delta_0, \quad n_3^0 = \sin\delta_0. \tag{11}$$

It was shown in Paper I that the accuracy of traveltime computations can be enhanced by calculating a correction along the first-order common S-wave ray. Although it is not strictly second-order traveltime correction, we refer to it as such, for the sake of simplicity. It reads

$$\Delta\tau^{[\mathcal{M}]} = \frac{1}{4} \int_{\tau_0}^{\tau} [c^{[\mathcal{M}]}(x_m, n_m)]^2 \frac{B_{13}^2(x_m, p_m) + B_{23}^2(x_m, p_m)}{V_P^2(x_m) - V_S^2(x_m)} d\tau. \tag{12}$$

Quantities B_{13} and B_{23} in eq. (12) are elements of the symmetric matrix $\mathbf{B}(x_m, p_m)$, see (7). Let us mention that the traveltime correction (12) does not depend on the choice of base vectors $\mathbf{e}^{[K]}$. The symbols V_S and V_P denote the S- and P-wave velocities of the reference isotropic medium, closely approximating the weakly anisotropic medium along the considered ray.

The first-order dynamic ray tracing (FODRT) system along the common ray of an S wave reads:

$$\begin{aligned}
\frac{dX_i^{(I)}}{d\tau} &= \frac{1}{2}\Big(\frac{\partial^2 G^{[\mathcal{M}]}(x_m, p_m)}{\partial p_i \partial x_j} X_j^{(I)} + \frac{\partial^2 G^{[\mathcal{M}]}(x_m, p_m)}{\partial p_i \partial p_j} Y_j^{(I)} \Big), \\
\frac{dY_i^{(I)}}{d\tau} &= -\frac{1}{2}\Big(\frac{\partial^2 G^{[\mathcal{M}]}(x_m, p_m)}{\partial x_i \partial x_j} X_j^{(I)} + \frac{\partial^2 G^{[\mathcal{M}]}(x_m, p_m)}{\partial x_i \partial p_j} Y_j^{(I)} \Big).
\end{aligned} \tag{13}$$

Here, $G^{[\mathcal{M}]}(x_m, p_m)$ is again the S-wave first-order mean eigenvalue given in eq. (4). Quantities $X_i^{(I)} = X_i^{(I)}(\tau)$ and $Y_i^{(I)} = Y_i^{(I)}(\tau)$ are defined as

$$X_i^{(I)} = [\frac{\partial x_i}{\partial \gamma^{(I)}}]_{\tau=const}, \quad Y_i^{(I)} = [\frac{\partial p_i}{\partial \gamma^{(I)}}]_{\tau=const}. \tag{14}$$

In (14), $\gamma^{(I)}$ again denote the ray parameters specifying the S-wave common ray, which can be chosen, for example, as in eq. (11). Quantities $X_i^{(I)}$ and $Y_i^{(I)}$ describe the variations along the wavefront of coordinates x_i of the first-order common ray and of components p_i of the first-order slowness vector caused by the variations of parameters $\gamma^{(I)}$. The FODRT equations can be used to calculate the first-order geometrical spreading $\mathcal{L}^{[\mathcal{M}]}(R, S)$ from source S to receiver R:

$$\mathcal{L}^{[\mathcal{M}]}(R, S) = |\mathbf{X}^{(1)} \times \mathbf{X}^{(2)}|^{1/2}. \tag{15}$$

The point-source initial conditions for the FODRT equations (13) for $\tau = \tau_0$ read:

$$X_i^{(I)}(\tau_0) = 0, \quad Y_i^{(I)}(\tau_0) = Z_{iI} - p_i^0 v_{0k}^{[\mathcal{M}]} Z_{kI}, \tag{16}$$

where

$$\begin{aligned} Z_{11} = -\sin\phi_0, \quad Z_{21} = \cos\phi_0, \quad Z_{31} = 0, \\ Z_{12} = -\cos\phi_0 \sin\delta_0, \quad Z_{22} = -\sin\phi_0 \sin\delta_0, \quad Z_{32} = \cos\delta_0, \end{aligned} \tag{17}$$

In eqs (16), $v_{0i}^{[\mathcal{M}]}$ denotes the ith component of the first-order ray-velocity vector of the common S wave, $v_i^{[\mathcal{M}]} = dx_i/d\tau$, at point S, at which $\tau = \tau_0$. Symbols ϕ_0 and δ_0 in eqs (17) again denote the take-off angles introduced in eq. (11).

The vectorial amplitude coefficient $\mathbf{U}(\tau)$ of the common S wave given in eq. (2), calculated along the S-wave common ray, reads:

$$\mathbf{U}(\tau) = \frac{\mathcal{A}_0(\tau)\mathbf{e}^{[1]}(\tau) + \mathcal{B}_0(\tau)\mathbf{e}^{[2]}(\tau)}{[\rho(\tau)c^{[\mathcal{M}]}(\tau)]^{1/2}\mathcal{L}^{[\mathcal{M}]}(\tau)}. \tag{18}$$

Parameter $\tau = \tau^{[\mathcal{M}]}(x_m)$ is again the first-order traveltime along the S-wave common ray, obtained by solving FORT equations (3). We choose vectors $\mathbf{e}^{[1]}$ and $\mathbf{e}^{[2]}$ as the base vectors of the wavefront orthogonal coordinate system (8). Frequency-dependent amplitude coefficients $\mathcal{A}_0$ and $\mathcal{B}_0$ can then be obtained by solving the system of coupled differential equations:

$$\begin{pmatrix} d\mathcal{A}_0/d\tau \\ d\mathcal{B}_0/d\tau \end{pmatrix} = -\frac{\mathrm{i}\omega}{2} \begin{pmatrix} B_{11} - 1 & B_{12} \\ B_{12} & B_{22} - 1 \end{pmatrix} \begin{pmatrix} \mathcal{A}_0 \\ \mathcal{B}_0 \end{pmatrix}. \tag{19}$$

In (19), B_{JL} are again the elements of the symmetric matrix $\mathbf{B}(x_m, p_m)$, see (7). Matrix $\mathbf{B}(x_m, p_m)$ can be obtained by simple rotation from matrix $\bar{\mathbf{B}}(x_m, p_m)$, specified explicitly in Paper I. Vectors $\mathbf{e}^{[K]}$ define the zero-order polarization plane of the common S wave. Thus the coupling equations (19) yield the vectorial amplitude coefficient $\mathbf{U}(\tau)$, which is situated in the zero-order polarization plane. From this reason, we call equations (19) *first-order coupling equations.*

If the wave field is generated by point force $\mathbf{F}$ acting at time $\tau = \tau_0$, the initial conditions for coupling equations (19) read:

$$\mathcal{A}_0(\tau_0) = \frac{e_k^{[1]}(\tau_0)F_k}{4\pi(\rho_0 c_0^{[\mathcal{M}]})^{1/2}}, \qquad \mathcal{B}_0(\tau_0) = \frac{e_k^{[2]}(\tau_0)F_k}{4\pi(\rho_0 c_0^{[\mathcal{M}]})^{1/2}}. \tag{20}$$

Here $c_0^{[\mathcal{M}]}$ denotes the first-order approximation of the S-wave common phase velocity at the source, and ρ_0 denotes the density at the same point.

In Paper I, the system of coupling equations (19) was derived under the assumption that another small parameter $\epsilon_2 \sim |\Delta a_{ijkl}|/|a_{ijkl}| \sim \Delta c/c$, characterizing weak anisotropy, is of the same order as the earlier introduced small parameter ϵ_1. Here, Δa_{ijkl} are perturbations of the density-normalized elastic parameters from the reference isotropic medium, Δc is the difference of the phase velocities of the two S waves propagating in the weakly anisotropic medium in the direction of slowness vector $\mathbf{p}$.

3 SECOND-ORDER COUPLING EQUATIONS

For greater accuracy of the results, it was proposed in Paper I to substitute vectors $\mathbf{e}^{[K]}$, which define the zero-order polarization plane of the common S wave, by their first-order counterparts $\mathbf{f}^{[K]}$:

$$\mathbf{f}^{[K]} = \mathbf{e}^{[K]} - (c^{[\mathcal{M}]})^2 \frac{B_{K3}(x_m, p_m)}{V_P^2 - V_S^2}\mathbf{e}^{[3]}. \tag{21}$$

Vectors $\mathbf{f}^{[K]}$ are situated in the plane perpendicular to the first-order eigenvector $\mathbf{f}^{[3]}$ corresponding to the largest eigenvalue of the generalized Christoffel matrix (5):

$$\mathbf{f}^{[3]} = (c^{[\mathcal{M}]})^2 \frac{B_{13}(x_m, p_m)}{V_P^2 - V_S^2}\mathbf{e}^{[1]} + (c^{[\mathcal{M}]})^2 \frac{B_{23}(x_m, p_m)}{V_P^2 - V_S^2}\mathbf{e}^{[2]} + \mathbf{e}^{[3]}. \tag{22}$$

Quantities B_{13}, B_{23} are again elements of matrix $\mathbf{B}(x_m, p_m)$, see (7). Symbols V_P and V_S denote the P- and S-wave velocities of the reference isotropic medium, also used in eq. (12).

After substitution of vectors $\mathbf{e}^{[K]}$ by $\mathbf{f}^{[K]}$ in (18), the zero-order vectorial amplitude coefficient $\mathbf{U}(\tau)$ reads:

$$\mathbf{U}(\tau) = \frac{\mathcal{A}_1(\tau)\mathbf{f}^{[1]}(\tau) + \mathcal{B}_1(\tau)\mathbf{f}^{[2]}(\tau)}{[\rho(\tau)c^{[\mathcal{M}]}(\tau)]^{1/2}\mathcal{L}^{[\mathcal{M}]}(\tau)}. \tag{23}$$

In (23), $\mathcal{A}_1$ and $\mathcal{B}_1$ are the amplitude coefficients, which we are seeking. Indices "1" should distinguish them from coefficients $\mathcal{A}_0$ and $\mathcal{B}_0$ used in (18). We can now proceed as in Paper I: insert eq. (23) into eq. (1), and the result into the elastodynamic equation, and neglect the terms of order $O(1), O(\omega^{-1})$ and less. Within this approximation, the substitution of vectors $\mathbf{e}^{[K]}$ by $\mathbf{f}^{[K]}$ only affects the coefficient of $(\mathrm{i}\omega)^2$ in eq. (31) of Paper

I. The effects on the coefficient of iω in eq. (31) can be neglected. Thus, if we take into account the definition of matrix $\mathbf{B}(x_m, p_m)$ in (7), eq. (32) of Paper I now reads:

$$(\Gamma_{ik}-\delta_{ik})C f_i^{[K]} f_k^{[L]} = C[B_{KL}-\delta_{KL}-2(c^{[\mathcal{M}]})^2\frac{B_{K3}B_{L3}}{V_P^2-V_S^2}+(c^{[\mathcal{M}]})^4(B_{33}-1)\frac{B_{K3}B_{L3}}{(V_P^2-V_S^2)^2}]. \quad (24)$$

This can be rewritten to read:

$$(\Gamma_{ik}-\delta_{ik})C f_i^{[K]} f_k^{[L]} = C(M_{KL}-\delta_{KL}). \quad (25)$$

The elements of the 2×2 matrix $\boldsymbol{M}$ in (25) read

$$M_{KL}(x_m, p_m) = B_{KL}(x_m, p_m) - (c^{[\mathcal{M}]})^2\frac{B_{K3}(x_m, p_m)B_{L3}(x_m, p_m)}{V_P^2-V_S^2}. \quad (26)$$

Matrix $\boldsymbol{M}$ was introduced in Farra (2001) and Farra and Pšenčík (2003) for calculating the second-order S-wave eigenvalues of the Christoffel matrix and of the corresponding first-order S-wave eigenvectors, which represent first-order polarization vectors. It is important to note that in deriving eq. (25), we choose velocities V_S and V_P in the following specific and unique way,

$$V_S^2(x_m) = (c^{[\mathcal{M}]})^2\ , \quad V_P^2(x_m) = (c^{[\mathcal{M}]})^2 B_{33}(x_m, p_m). \quad (27)$$

Eq. (27) yields $B_{33}-1 = (c^{[\mathcal{M}]})^{-2}(V_P^2-V_S^2)$. Eq.(26) can thus be rewritten to the alternative form

$$M_{KL}(x_m, p_m) = B_{KL}(x_m, p_m) - \frac{B_{K3}(x_m, p_m)B_{L3}(x_m, p_m)}{B_{33}(x_m, p_m)-1}, \quad (28)$$

which is independent of the reference medium. Note that the element B_{33} of the matrix $\mathbf{B}$ represents the first-order approximation of the largest of the eigenvalues of the Christoffel matrix (5). The coupled system of differential equations (19) then transforms into the system:

$$\begin{pmatrix} d\mathcal{A}_1/d\tau \\ d\mathcal{B}_1/d\tau \end{pmatrix} = -\frac{\mathrm{i}\omega}{2}\begin{pmatrix} M_{11}-1 & M_{12} \\ M_{12} & M_{22}-1 \end{pmatrix}\begin{pmatrix} \mathcal{A}_1 \\ \mathcal{B}_1 \end{pmatrix}. \quad (29)$$

We call equations (29) *second-order coupling equations*. They are obtained from the first-order coupling equations (19) just by substituting the elements B_{11}, B_{12} and B_{22} of matrix $\boldsymbol{B}$ by the elements M_{11}, M_{12} and M_{22} of matrix $\boldsymbol{M}$. In Appendix A, we show that the substitution of eqs (19) by (29) leads to the increase of accuracy of the computed traveltimes $\tau_{S1,S2}$ along the S-wave common ray. The computed traveltimes $\tau_{S1,S2}$ contain, for example, the second-order traveltime correction (12). We illustrate this fact also on numerical examples.

The initial conditions have a form similar to those in (20). Only vectors $\mathbf{e}^{[K]}$ are substituted by vectors $\mathbf{f}^{[K]}$:

$$\mathcal{A}_1(\tau_0) = \frac{f_k^{[1]}(\tau_0)F_k}{4\pi(\rho_0 c_0^{[\mathcal{M}]})^{1/2}}, \qquad \mathcal{B}_1(\tau_0) = \frac{f_k^{[2]}(\tau_0)F_k}{4\pi(\rho_0 c_0^{[\mathcal{M}]})^{1/2}}. \quad (30)$$

4 NUMERICAL EXAMPLES

In order to illustrate the accuracy of the first-order and second-order coupling equations we consider the VSP configuration, which we used in our previous studies of FORT and FODRT for P waves, see Pšenčík & Farra (2005, 2007). The source and the borehole are situated in a vertical plane (x, z). The borehole is parallel to the z axis, the vertical single-force source is located on the surface at $z = 0$ km, at a distance of 1 km from the borehole. The source-time function is a windowed symmetric Gabor wavelet, $\exp[-(2\pi f/\gamma)^2 2t^2]\cos(2\pi f t)$, with the dominant frequency $f = 50$ Hz and $\gamma = 4$. There are 29 three-component receivers in the borehole, distributed with a uniform step of 0.02 km, with receiver depths ranging from 0.01 to 0.57 km. The receivers record the vertical (positive downwards), transverse and radial (along the line connecting the source and the top of the borehole; positive away from the source) components of the wave field. The recording system is right-handed. All calculated seismograms are shown with no differential scaling between components and traces, so that true relative amplitudes can be seen.

We consider three models, QI, QI2 and QI4, used by Klimeš & Bulant (2004) and Bulant & Klimeš (2008). Model QI coincides with the WA model of Pšenčík & Dellinger (2001). The models are vertically inhomogeneous HTI media with constant vertical gradients of the elastic moduli. The axis of symmetry is rotated everywhere in the horizontal plane by 45^o from the vertical plane (x, z). The S-wave anisotropy defined as $(c_{S1} - c_{S2})/c_{average} \times 100\%$ ranges, from the horizontal to vertical direction, from 1% to 4%, from 4% to 7% and from 11% to 13% for the QI, QI2 and QI4 models, respectively. The matrices of the density-normalized elastic moduli can be found in the above references. The variations of the S-wave phase velocities in the (x, z) plane for all three models are shown in Fig. 1. The left-hand plots correspond to $z = 0$ km, the right-hand plots to $z = 1$ km. Model QI is shown in the top, QI2 in the middle and QI4 in the bottom plot. Velocities are shown as functions of the angle of incidence. They vary from 0^0 (horizontal propagation) to 90^0 (vertical propagation). Although the coupling method based on the FORT can accommodate arbitrary lateral variations of the elastic moduli, the models used exhibit only vertical variations.

In addition to inhomogeneous QI, QI2 and QI4 models, we also consider their homogeneous counterparts specified by the elastic parameters of the above models at $z = 0$ km. The homogeneous models are thus represented by the plots in the left-hand column of Fig. 1. We call these models QI HOM, QI2 HOM and QI4 HOM. Since there is no coupling in homogeneous media (the two S waves are decoupled there), homogeneous models allow us to investigate the accuracy of the traveltime and spreading approximations.

Figure 2 shows the relative traveltime and geometrical-spreading differences for the homogeneous QI2 HOM model. The relative difference of quantity q is computed as

$$\frac{q_{FORT} - q_{EXACT}}{q_{EXACT}} \times 100\%. \tag{31}$$

Quantity q_{FORT} is obtained along the common S-wave ray. Quantity q_{EXACT} is computed along rays of S1 and S2 waves, by the ray tracer for anisotropic media – a modified program package ANRAY (Gajewski and Pšenčík, 1990) which is based on the standard ray theory. Blue corresponds to the faster S1 wave, red to the slower S2 wave. Black corresponds to

their average. In contrast to similar figures shown in Pšenčík & Farra (2005, 2007), the plots for S1 and S2 waves in Fig.2 do not show relative errors. They only show deviations of traveltimes and spreading computed along a common S-wave ray from these quantities computed exactly along the rays of the S1 and S2 waves. Only the differences between FORT quantities and averages of exact quantities can be considered as relative errors, because the values q_{FORT} represent approximations of averaged quantities. In the upper plot of Fig.2, quantity q_{FORT} is the traveltime $\tau^{[\mathcal{M}]}$ obtained by solving FORT equations (3) along the common S-wave ray. In the middle plot, the traveltime $\tau^{[\mathcal{M}]}$ is corrected by term $\Delta\tau^{[\mathcal{M}]}$ from eq. (12), which we briefly call a second-order correction. In the bottom plot of Fig.2, quantity q_{FORT} is the first-order geometrical spreading $\mathcal{L}^{[\mathcal{M}]}$. The V_S and V_P velocities in eq. (12) are determined according to eq. (27).

We can see that the deviations of the first- and second-order traveltimes, computed along the common S-wave ray, from the traveltimes of each of the S waves are less than 2%. The deviation of the first-order traveltimes related to the S1 wave is less than that related to the S2 wave. The relative error of the first-order traveltime with respect to the averaged exact traveltime is about 1%. This error is reduced to nearly zero if the second-order traveltime correction (12) is used (black symbols in the middle plot). The deviations of the second-order traveltimes from the S1- and S2-wave traveltimes are comparable, but with opposite sign, in this case. As in the case of the P waves, we can see that the first-order geometrical spreading (black) is less accurate than the traveltime. The relative error with respect to the averaged spreading is approximately -3%. Note that the first-order geometrical spreading $\mathcal{L}^{[\mathcal{M}]}$, computed along the common S-wave ray, is smaller than the spreading of each of the two S waves (the relative differences, red and blue, are negative).

In Figure 3, we compare the synthetic seismograms, computed from the first-order coupling equations (19) (red) and the standard ray theory seismograms (black) in the QI2 HOM model. The red seismograms are plotted over the black ones in this and the following comparisons. We can see that the faster S1 wave (observable in the vertical component and, for deeper receivers, also on the transverse component) is relatively well approximated by equations (19). The approximation of the S2 wave is worse. We can see a very poor fit of the approximate seismograms in the radial and transverse components, especially for deeper receivers. This is the consequence of the traveltime approximation incorporated in eqs (19), see eq. (A5) in Appendix A. The discrepancies between the approximate and standard ray theory seismograms (black) are removed, if the approximate seismograms (red) are computed from the second-order coupling equations (29), see Fig. 4. This is the consequence of the use of a better traveltime approximation, see eq. (A12) in Appendix A. We can see that the second-order coupling equations (29) (red) yield a good fit with the standard ray theory seismograms (black) even for model QI4 HOM with the S-wave anisotropy between 11%-13%, shown in Fig. 5. The S1 wave computed by equations (29) is slightly faster and has a slightly overestimated amplitude with respect to the S1 wave computed by the standard ray method. The larger amplitude is the consequence of the relative difference (31) of the S1-wave spreading being about -11% in this case. Let us emphasize that the two well separated S waves shown in red in Fig. 5 are computed along a *single* common S-wave ray.

Let us now consider QI models with vertical inhomogeneity, in which we can observe coupling effects. We do not show the plots of the relative differences of the first- and second-order traveltimes and of the geometrical spreading. For model QI2, they differ

only a little from the plots shown in Fig. 2.

In Fig. 6, we show the comparison of the seismograms computed from the first-order coupling equations (19) (black) and from the second-order coupling equations (29) (red). For the faster S1 wave (mostly observable in the vertical and radial components), we have a nearly perfect fit of both approximations. For the S2 wave (mostly observable in the transverse component), we can observe certain differences. The S2 wave computed by the first-order coupling equations is slightly faster than the S2 wave computed by the second-order coupling equations.

As mentioned above, model QI is identical with model WA studied by Pšenčík & Dellinger (2001). They used the quasi-isotropic approximation with a common S-wave ray traced in a reference isotropic medium and compared the results with the results computed by the reflectivity method. In Fig. 7, we compare the seismograms computed by the second-order coupling equations (29) (red) with the seismograms computed by the quasi-isotropic approach (black). No amplitude normalization (which had to be used by Pšenčík & Dellinger, 2001) is used. Except for the slightly higher amplitudes of both S waves computed by the quasi-isotropic approach, the comparison resembles the comparison of the seismograms, computed from the first-order and second-order coupling equations, shown in Fig. 6. The S2 wave computed by the quasi-isotropic approach is slightly faster than the S2 wave computed by the second-order coupling equations.

Since the anisotropy of the QI model is relatively weak, the results of the quasi-isotropic approach and the first-order and second-order coupling equations presented in this paper are comparable. Let us now compare the seismograms computed by the second-order coupling equations (29) (red) with the standard ray theory seismograms computed by the package ANRAY. Fig. 8 shows this comparison. We can see the nearly perfect fit of the S1 wave, observable again mostly in the vertical and radial components, except for the slightly higher amplitudes computed by ANRAY at deeper receivers, but a strong misfit of the S2 wave, mostly observable in the transverse component. The most pronounced differences, mainly due to the phase shift, can be seen at the shallow receivers. This misfit indicates the failure of the standard ray theory (used in the ANRAY package) to describe properly the phenomenon of coupling.

Let us now consider the stronger anisotropy, specifically model QI2. Similarly as in Fig. 6, we compare the results of the computations based on the first-order coupling equations (19) (black) with those based on the second-order coupling equations (29) (red) in Fig. 9. While in Fig. 6 both equations yielded comparable results, in the medium with stronger anisotropy their results differ. The most dramatic difference (both in phase shift and amplitude) can be observed for the S2 wave. The differences are so pronounced that they can be observed in all three components, mostly in the transverse. As superior, we consider, of course, the seismograms computed using eqs (29). In contrast to the first-order coupling equations, eqs (29) describe, specifically for the deeper receivers in the transverse component, the separation of the S1 and S2 waves.

The separation of the S1 and S2 waves is visible more clearly in Fig. 10, which shows the same comparison as Fig. 8. Specifically, Fig. 10 compares the seismograms, computed by the second-order coupling equations (29) (red), with the standard ray theory seismograms computed by the ANRAY package. We can see that the fit is now much better than in Fig. 8. This is because the anisotropy is now sufficiently strong so that

the coupling effects are not as pronounced (the coupling still affects wave field at shallow receivers). In the transverse component, we can observe very clear separation of the S1 and S2 waves.

Figure 11 shows the same as Fig.10, but for the QI4 model. We can now observe clear separation (of about 0.06 sec; approximately three wave periods) of the two S waves in all components. The fit is not as good as in Fig. 10. The S1 wave computed from equations (29) is slightly faster and has a slightly overestimated amplitude with respect to the S1 wave computed by the standard ray method, see a similar observation in Fig. 5. Let us emphasize again that, while the two well-separated S waves shown in black in Fig. 11 are calculated each along a different S-wave ray, the S waves shown in red in Fig. 11 are computed along a *single* common S-wave ray.

5 DISCUSSION AND CONCLUSIONS

We have generalized approximate coupling equations for computing the coupled S waves propagating in smooth inhomogeneous, weakly anisotropic media, proposed in Paper I. The generalization consists in substituting two mutually perpendicular unit vectors, which define the zero-order polarization plane of the common S wave in Paper I by vectors, which define the polarization plane more accurately. The generalization leads to a substantial increase in the accuracy of the computed S-wave field as illustrated by numerical examples.

The proposed procedure is applicable to the S waves propagating in inhomogeneous, isotropic or weakly anisotropic media of arbitrary symmetry. In isotropic media, it reduces to exact ray tracing and dynamic ray tracing. Equations (8) reduce to the equations for the vector base of the ray-centred coordinate system, in which the vectors $\mathbf{e}^{[K]}$ specify the polarization vectors of the S wave propagating in an inhomogeneous isotropic medium. In anisotropic media, the proposed procedure can deal with coupled as well as decoupled S waves. The common S-wave ray tracing is regular everywhere including singular regions.

The second-order coupling equations have a simple and transparent form. They differ from the first-order coupling equations only by the substitution of elements B_{11}, B_{12} and B_{22} of matrix $\mathbf{B}$ by elements M_{11}, M_{12} and M_{22} of matrix $\mathbf{M}$. Computation of elements of matrix $\mathbf{M}$ is simple and does not require much extra computational effort. The second-order coupling equations contain the corrections of the common S-wave traveltime implicitly. Simple, approximate formulae for traveltimes of separate S waves can be obtained as a byproduct of the coupling procedure. These formulae may find applications in migration and traveltime tomography based on S waves. The coupling procedure described in this paper can be simply generalized for laterally varying, layered, weakly anisotropic structures.

The computations of common S-wave rays and of dynamic ray tracing along them are based on FORT and FODRT (Pšenčík & Farra, 2005, 2007). The coupling equations are also approximate, based on perturbation formulae. Despite this, the proposed scheme generates quite accurate results; compare the results presented in this paper with the results of Bulant & Klimeš (2008). The scheme proposed in this paper also provides

satisfactory results for decoupled S waves as shown in the comparisons with the results of the standard ray theory for anisotropic media.

As the next step, we plan to study the behaviour of the proposed procedure in more complicated models. We plan to concentrate specifically on S-wave computations close to singularities. We also plan to test the accuracy of the traveltime formulae given in Appendix A.

ACKNOWLEDGEMENTS

A substantial part of this work was done during IP's stay at the IPG Paris at the invitation of the IPGP. We appreciate the useful discussions with Einar Iversen and his comments. We are grateful to the Consortium Project "Seismic waves in complex 3-D structures" (SW3D) and Research Project 205/08/0332 of the Grant Agency of the Czech Republic for support.

REFERENCES

Bakker, P., 2002. Coupled anisotropic shear-wave ray tracing in situations where associated slowness sheets are almost tangent, *Pure Appl. Geophys.*, **159**, 1403–1417.

Bulant, P. & Klimeš, L., 2002. Numerical algorithm of the coupling ray theory in weakly anisotropic media, *Pure Appl. Geophys.*, **159**, 1419–1435.

Bulant, P. & Klimeš, L., 2008. Numerical comparison of the isotropic- common-ray and anisotropic-common-ray approximations of the coupling ray theory, *Geophys. J. Int.*, **175**, 357–374.

Červený, V., 2001. *Seismic Ray Theory*, Cambridge Univ. Press, Cambridge.

Coates, R.T. & Chapman, C.H., 1990. Quasi–shear wave coupling in weakly anisotropic 3-D media, *Geophys. J. Int.*, **103**, 301–320.

Farra, V. 2001. High order expressions of the phase velocity and polarization of qP and qS waves in anisotropic media, *Geophys. J. Int.*, **147**, 93-105.

Farra, V., & Pšenčík, I., 2003. Properties of the zero-, first- and higher-order approximations of attributes of elastic waves in weakly anisotropic media, *J. Acoust. Soc. Am.*, **114**, 1366–1378.

Farra, V. & Pšenčík, I., 2008. First-order ray computations of coupled S waves in inhomogeneous weakly anisotropic media, *Geophys. J. Int.*, **173**, 979–989.

Gajewski, D., & Pšenčík, I., 1990. Vertical seismic profile synthetics by dynamic ray tracing in laterally varying layered anisotropic structures, *J. Geophys. Res.*, **95**, 11301–11315.

Klimeš, L., 2006. Common-ray tracing and dynamic ray tracing for S waves in a

smooth elastic anisotropic medium, *Stud. Geophys. Geod.*, **50**, 449–461.

Klimeš, L. & Bulant, P., 2004. Errors due to the common ray approximations of the coupling ray theory, *Stud. Geophys. Geod.*, **48**, 117–142.

Kravtsov, Yu.A., 1968. "Quasiisotropic" approximation to geometrical optics, *Dokl. AN SSSR*, **183**, No.1, 74-77 (in Russian).

Kravtsov, Yu.A. & Orlov,Yu.I., 1990. *Geometrical Optics of Inhomogeneous Media*, Springer–Verlag, Heidelberg.

Pšenčík, I., 1998. Green's functions for inhomogeneous weakly anisotropic media, *Geophys. J. Int.*, **135**, 279–288.

Pšenčík,I. & Dellinger.J., 2001. Quasi-shear waves in inhomogeneous weakly anisotropic media by the quasi-isotropic approach: a model study, *Geophysics*, **66**, 308–319.

Pšenčík, I., & Farra, V., 2005. First-order ray tracing for qP waves in inhomogeneous weakly anisotropic media, *Geophysics*, **70**, D65–D75.

Pšenčík, I. & Farra,V., 2007. First-order P-wave ray synthetic seismograms in inhomogeneous weakly anisotropic media. *Geophys. J. Int.*, **170**, 1243–1252.

Thomson, C.J., Kendall, J-M. & Guest, W.S., 1992. Geometrical theory of shear wave splitting: corrections to ray theory for interference in isotropic/anisotropic transitions. *Geophys. J. Int.*, **108**, 339–363.

Vavryčuk, V., 2003. Behavior of rays near singularities in anisotropic media. *Phys. Rev.*, **B 67**, 054 105-1 – 054 105-8.

APPENDIX A: SPECIAL SITUATIONS

In Paper I, the first-order S-wave coupling equations were derived under the assumption that the two small parameters $\epsilon_1 \sim c/(\omega L)$ and $\epsilon_2 \sim |\Delta c|/c$ are of the same order, $\epsilon_1 \sim \epsilon_2$. Let us consider other possible situations.

In isotropic media, i.e. for $\epsilon_2 = 0$, equations (19) yield $\mathcal{A}_0 = const$, $\mathcal{B}_0 = const$. If we insert this into eq.(18), and the result into equation (1), we obtain the well-known zero-order ray expression for the displacement vector $\mathbf{u}$ of an S wave propagating in an inhomogeneous isotropic medium. The vectors $\mathbf{e}^{[K]}$ computed from eq.(8) represent the S-wave polarization vectors.

For stronger anisotropy (Δc larger), higher frequencies (ω large) or weaker inhomogeneity, including homogeneity (characteristic length L large or infinite), i.e. for the case $\epsilon_1 \ll \epsilon_2$, the coupling is expected to be weaker and we can thus seek solutions of the coupled equations (19) in the following form (Pšenčík 1998):

$$\mathcal{A}_0(\tau) = \mathcal{A}'_0 \exp(\mathrm{i}\omega\Delta\tau), \qquad \mathcal{B}_0(\tau) = \mathcal{B}'_0 \exp(\mathrm{i}\omega\Delta\tau). \tag{A1}$$

Here $\mathcal{A}'_0$ and $\mathcal{B}'_0$ are the amplitude factors, $\Delta\tau$ are deviations of the traveltimes from the first-order traveltime $\tau^{[\mathcal{M}]}$ calculated along the common S-wave ray. Inserting (A1) into eq.(19) and considering $\epsilon_1 \ll \epsilon_2$, we arrive at $d\mathcal{A}'_0/\tau \sim 0$, $d\mathcal{B}'_0/\tau \sim 0$ and:

$$2\frac{d\Delta\tau}{d\tau}\begin{pmatrix} \mathcal{A}'_0 \\ \mathcal{B}'_0 \end{pmatrix} + \begin{pmatrix} B_{11}-1 & B_{12} \\ B_{12} & B_{22}-1 \end{pmatrix}\begin{pmatrix} \mathcal{A}'_0 \\ \mathcal{B}'_0 \end{pmatrix} = 0. \tag{A2}$$

Eq.(A2) can be expressed in the form of an eigenvalue problem:

$$\begin{pmatrix} B_{11}-(1-2d\Delta\tau/d\tau) & B_{12} \\ B_{12} & B_{22}-(1-2d\Delta\tau/d\tau) \end{pmatrix}\begin{pmatrix} \mathcal{A}'_0 \\ \mathcal{B}'_0 \end{pmatrix} = 0. \tag{A3}$$

Eq.(A3) represents a system of two equations for two eigenvalues $1-2d\Delta\tau/d\tau$ and two corresponding eigenvectors situated in the plane specified by vectors $\mathbf{e}^{[K]}$. The two eigenvalues and corresponding eigenvectors correspond to two independent S waves that we call S1 and S2 in the following. From the eigenvalues of eq.(A3), we get

$$\frac{d\Delta\tau}{d\tau} = \frac{1}{2} - \frac{1}{4}[(B_{11}+B_{22}) \pm \sqrt{(B_{11}-B_{22})^2+4B_{12}^2}. \tag{A4}$$

Taking into account that $B_{11}(x_m,p_m) + B_{22}(x_m,p_m) = 2$, see eqs (4) and (9), we can use (A4) in the expression for the approximate traveltimes τ_{S1} and τ_{S2} of the S waves, between points corresponding to τ_0 and τ on the common S-wave ray:

$$\tau_{S1,S2}(\tau,\tau_0) = \tau^{[\mathcal{M}]}(\tau,\tau_0) + \Delta\tau_{S1,S2}(\tau,\tau_0)\ . \tag{A5}$$

The term $\tau^{[\mathcal{M}]}(\tau,\tau_0)$ is the first-order traveltime calculated between points corresponding to τ_0 and τ on the common S-wave ray. If the common S-wave ray does not pass through a singularity, the term $\Delta\tau_{S1,S2}$, which represents deviations of the traveltimes of S1 and S2 waves from $\tau^{[\mathcal{M}]}(\tau,\tau_0)$, has the following meaning:

$$\Delta\tau_{S1} = -\frac{1}{4}\int_{\tau_0}^{\tau} \sqrt{(B_{11}-B_{22})^2+4B_{12}^2}\ d\tau,$$

$$\Delta\tau_{S2} = \frac{1}{4}\int_{\tau_0}^{\tau} \sqrt{(B_{11}-B_{22})^2 + 4B_{12}^2}\; d\tau. \qquad (A6)$$

In this way, the S1 wave is faster than the S2 wave. The zero value of the argument of the integrals in eq.(A6) indicates either a singularity or S-wave propagation in an isotropic medium. The approximate traveltime difference of the S1 and S2 waves is thus $\frac{1}{2}\int_{\tau_0}^{\tau} \sqrt{(B_{11}-B_{22})^2 + 4B_{12}^2}\; d\tau$. Since the difference is related to the first-order traveltime calculated along the common ray, we call it the *first-order traveltime difference*.

The eigenvectors of equation (A3) specify the directions of the zero-order polarization vectors of the two decoupled waves. We can introduce the polarization vectors $\mathbf{e}^{'[K]}$ as unit, mutually orthogonal vectors situated in the plane specified by vectors $\mathbf{e}^{[K]}$, see eq.(8). At any point of the common S-wave ray, the vectors $\mathbf{e}^{'[K]}$ are given by the expressions:

$$\mathbf{e}^{'[1]} = \mathbf{e}^{[1]} cos\Phi_0 + \mathbf{e}^{[2]} sin\Phi_0, \qquad \mathbf{e}^{'[2]} = -\mathbf{e}^{[1]} sin\Phi_0 + \mathbf{e}^{[2]} cos\Phi_0. \qquad (A7)$$

Angle Φ_0 is the angle, which leads to the diagonalization of the matrix on the left-hand side of eq.(A3). In other words, rotation through angle Φ_0 changes the matrix $\mathbf{B}$ into $\mathbf{B}'$, in which $B'_{12} = 0$. From this condition we get (Pšenčík, 1998; Farra, 2001; Farra & Pšenčík, 2003):

$$\tan 2\Phi_0 = \frac{2B_{12}}{B_{11}-B_{22}}. \qquad (A8)$$

Angle Φ_0 has been chosen so that vector $\mathbf{e}^{'[1]}$ corresponds to the S1 wave. The polarization vector $\mathbf{e}^{'[2]}$ corresponds to the S2 wave.

We can now rewrite eq.(18) in the following form:

$$\mathbf{U}(\tau) = \frac{\mathcal{D}'_0 \mathbf{e}^{'[1]}(\tau)\exp(\mathrm{i}\omega\Delta\tau_{S1}) + \mathcal{F}'_0 \mathbf{e}^{'[2]}(\tau)\exp(\mathrm{i}\omega\Delta\tau_{S2})}{[\rho(\tau)c^{[\mathcal{M}]}(\tau)]^{1/2}\mathcal{L}^{[\mathcal{M}]}(\tau)}. \qquad (A9)$$

In (A9), $\mathcal{D}'_0$ and $\mathcal{F}'_0$ are factors constant along the ray, which can be expressed in terms of the factors $\mathcal{A}'_0$ and $\mathcal{B}'_0$, given in (A1), in the following way:

$$\mathcal{D}'_0 = \mathcal{A}'_0 cos\Phi_0(\tau_0) + \mathcal{B}'_0 sin\Phi_0(\tau_0), \qquad \mathcal{F}'_0 = -\mathcal{A}'_0 sin\Phi_0(\tau_0) + \mathcal{B}'_0 cos\Phi_0(\tau_0). \qquad (A10)$$

The factors $\mathcal{A}'_0$, $\mathcal{B}'_0$ can be determined from the initial conditions, the angle $\Phi_0(\tau_0)$ from eq.(A8) applied at $\tau = \tau_0$. The traveltime deviations $\Delta\tau_{S1}$, $\Delta\tau_{S2}$ are given in (A6), the polarization vectors $\mathbf{e}^{'[K]}$ in (A7). After inserting eq.(A9) into eq.(1), eq.(1) describes two decoupled S waves. Each of them is given in the form of the zero-order ray expression for the displacement vector $\mathbf{u}$ of an S wave propagating in an inhomogeneous anisotropic medium. Both waves share the same spreading factor, but they differ by their polarizations and traveltimes, see eq.(A9). The wave specified by the factor $\mathcal{D}'_0$ and the polarization vector $\mathbf{e}^{'[1]}$ is the S1 wave, the other is the S2 wave. Note that for the evaluation of (A9), it is only necessary to solve FORT and FODRT equations together with eq.(8) for the vectorial base of the wavefront orthonormal coordinate system as in the case of computations of separate waves. In addition, it is, however, also necessary to evaluate the deviations $\Delta\tau_{S1,S2}$ from eqs (A6). There is no need to solve the coupling equations (19).

Similarly as in eq.(A1), we can seek the solution of the second-order coupling equations (29) in the form:

$$\mathcal{A}_1(\tau) = \mathcal{A}'_1 \exp(\mathrm{i}\omega\Delta\tau), \qquad \mathcal{B}_1(\tau) = \mathcal{B}'_1 \exp(\mathrm{i}\omega\Delta\tau). \qquad (A11)$$

Inserting (A11) into eqs (29) and considering $\epsilon_1 \ll \epsilon_2$, we arrive at $d\mathcal{A}_1'/\tau \sim 0$, $d\mathcal{B}_1'/\tau \sim 0$ and:

$$2\frac{d\Delta\tau}{d\tau}\begin{pmatrix}\mathcal{A}_1'\\ \mathcal{B}_1'\end{pmatrix}+\begin{pmatrix}M_{11}-1 & M_{12}\\ M_{12} & M_{22}-1\end{pmatrix}\begin{pmatrix}\mathcal{A}_1'\\ \mathcal{B}_1'\end{pmatrix}=0. \qquad (A12)$$

As in case of eq.(A2), we can consider (A12) as an eigenvalue problem for eigenvalues $1-2d\Delta\tau/d\tau$ and the corresponding eigenvectors situated in the plane specified by vectors $\mathbf{f}^{[K]}$. From the eigenvalues we can find

$$\frac{d\Delta\tau}{d\tau}=\frac{1}{2}-\frac{1}{4}[(M_{11}+M_{22})\pm\sqrt{(M_{11}-M_{22})^2+4M_{12}^2}\,]. \qquad (A13)$$

Using eq.(26) and again taking into account that $B_{11}(x_m,p_m)+B_{22}(x_m,p_m)=2$, we get

$$M_{11}+M_{22}=2-(c^{[\mathcal{M}]})^2\frac{B_{13}^2+B_{23}^2}{V_P^2-V_S^2}. \qquad (A14)$$

Using eq.(A14), and assuming that the common S-wave ray does not pass through a singularity, we can use eq.(A13) in the expressions for the approximate traveltimes τ_{S1} and τ_{S2} of faster S1 and slower S2 waves between points corresponding to τ_0 and τ on the common S-wave ray:

$$\tau_{S1,S2}(\tau,\tau_0)=\tau^{[\mathcal{M}]}(\tau,\tau_0)+\Delta\tau_{S1,S2}(\tau,\tau_0)\ . \qquad (A15)$$

The term $\tau^{[\mathcal{M}]}(\tau,\tau_0)$ is the first-order traveltime calculated between points corresponding to τ_0 and τ on the common S-wave ray. The term $\Delta\tau_{S1,S2}$ has now the following meaning:

$$\Delta\tau_{S1}=\Delta\tau^{[\mathcal{M}]}-\frac{1}{4}\int_{\tau_0}^{\tau}\sqrt{(M_{11}-M_{22})^2+4M_{12}^2}\ d\tau,$$

$$\Delta\tau_{S2}=\Delta\tau^{[\mathcal{M}]}+\frac{1}{4}\int_{\tau_0}^{\tau}\sqrt{(M_{11}-M_{22})^2+4M_{12}^2}\ d\tau. \qquad (A16)$$

The term $\Delta\tau^{[\mathcal{M}]}$ is the second-order traveltime correction given in eq.(12). We can see that the second-order traveltime correction is automatically incorporated in the coupling equations (29). The second terms on the right-hand sides of eqs (A16) control separation of S waves. The approximate traveltime difference of the S1 and S2 waves is now $\frac{1}{2}\int_{\tau_0}^{\tau}\sqrt{(M_{11}-M_{22})^2+4M_{12}^2}\ d\tau$. Since it is related to the expressions, which contain second-order traveltime corrections calculated along the common ray, we call (A16) the *second-order traveltime difference.*

Comparing eqs (A15) and (A16) with (A5) and (A6), we can see that the increased accuracy of (A15) is caused by two effects. First, by the second-order traveltime correction $\Delta\tau^{[\mathcal{M}]}$ and second, by the more accurate traveltime difference, see the second term on the right-hand sides of eqs (A16).

The eigenvectors of eq.(A12) specify the direction of the first-order polarization vectors $\mathbf{f}'^{[K]}$ of the two decoupled waves. They are situated in the plane specified by vectors $\mathbf{f}^{[K]}$, see eq.(21); at any point of the common S-wave ray, the vectors $\mathbf{f}'^{[K]}$ can be expressed as follows:

$$\mathbf{f}'^{[1]}=\mathbf{f}^{[1]}cos\Phi_1+\mathbf{f}^{[2]}sin\Phi_1,\qquad \mathbf{f}'^{[2]}=-\mathbf{f}^{[1]}sin\Phi_1+\mathbf{f}^{[2]}cos\Phi_1. \qquad (A17)$$

The polarization vectors $\mathbf{f}'^{[K]}$ are not unit since vectors $\mathbf{f}^{[K]}$ are also not unit. Angle Φ_1 is specified so that the element M'_{12} of the rotated matrix $\mathbf{M}$ equals zero, $M'_{12} = 0$. This condition yields (Farra, 2001; Farra & Pšenčík, 2003):

$$\tan 2\Phi_1 = \frac{2M_{12}}{M_{11} - M_{22}}. \qquad (A18)$$

Angle Φ_1 has been chosen so that vector $\mathbf{f}'^{[1]}$ corresponds to the S1 wave. The polarization vector $\mathbf{f}'^{[2]}$ corresponds to the S2 wave.

We can now rewrite eq.(23) in the following form:

$$\mathbf{U}(\tau) = \frac{\mathcal{D}'_1 \mathbf{f}'^{[1]}(\tau)\exp(\mathrm{i}\omega\Delta\tau_{S1}) + \mathcal{F}'_1 \mathbf{f}'^{[2]}(\tau)\exp(\mathrm{i}\omega\Delta\tau_{S2})}{[\rho(\tau)c^{[\mathcal{M}]}(\tau)]^{1/2}\mathcal{L}^{[\mathcal{M}]}(\tau)}. \qquad (A19)$$

In (A19), $\mathcal{D}'_1$ and $\mathcal{F}'_1$ are factors constant along the ray, which can be expressed in terms of the factors $\mathcal{A}'_1$ and $\mathcal{B}'_1$ given in (A11) in the following way:

$$\mathcal{D}'_1 = \mathcal{A}'_1 cos\Phi_1(\tau_0) + \mathcal{B}'_1 sin\Phi_1(\tau_0), \qquad \mathcal{F}'_1 = -\mathcal{A}'_1 sin\Phi_1(\tau_0) + \mathcal{B}'_1 cos\Phi_1(\tau_0). \qquad (A20)$$

The factors $\mathcal{A}'_1$, $\mathcal{B}'_1$ can be determined from the initial conditions, the angle $\Phi_1(\tau_0)$ from eq.(A18) applied at $\tau = \tau_0$. The terms $\Delta\tau_{S1}$, $\Delta\tau_{S2}$ are given in (A16), the polarization vectors $\mathbf{f}'^{[K]}$ in (A17). We can see from eq.(A19) that, for $\epsilon_1 \ll \epsilon_2$, also the second-order coupling equations yield two separate S waves with the same spreading factor, but different polarizations and traveltimes.

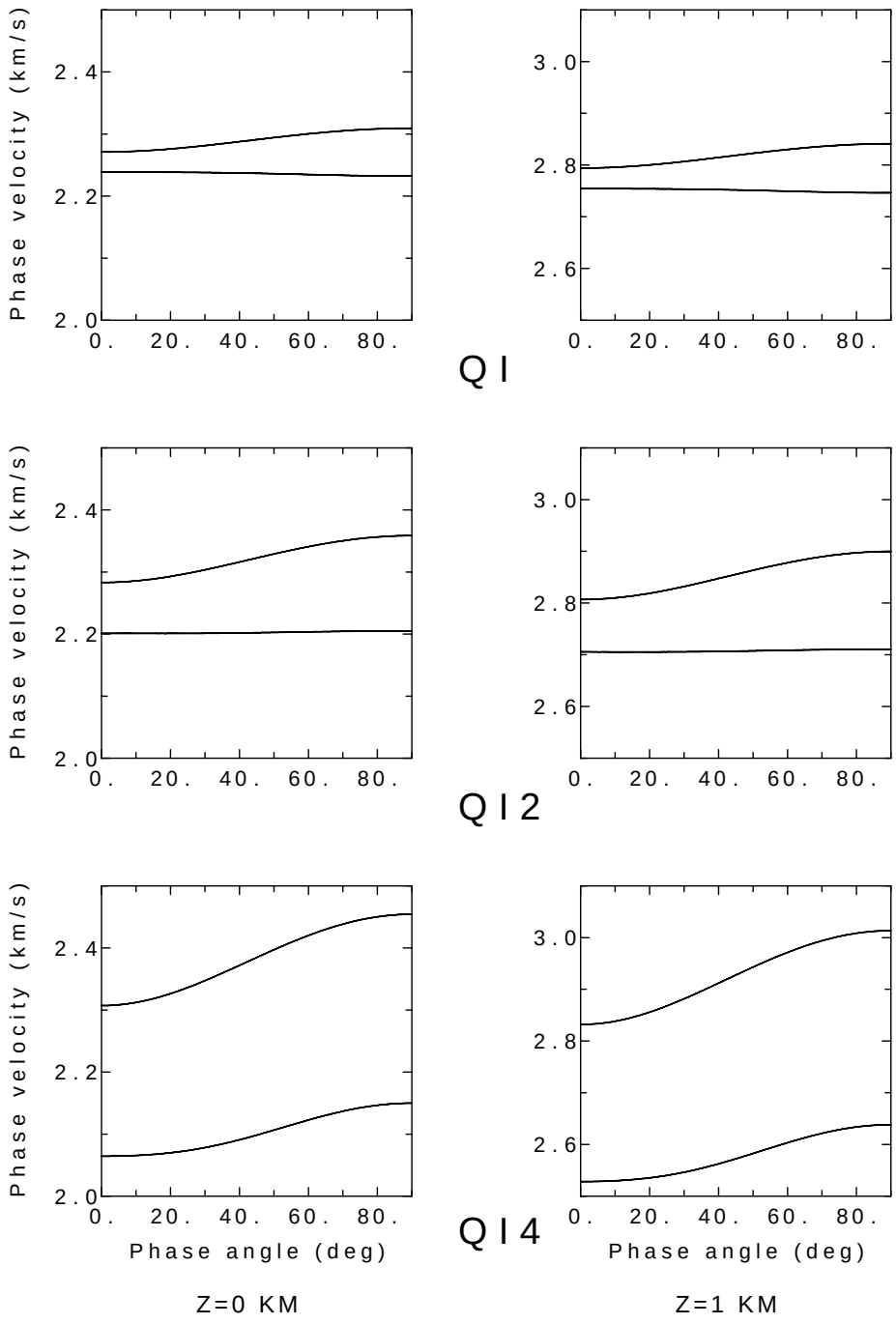

Figure 1: The S-wave phase-velocity sections in the (x, z) plane for models QI (top), QI2 (middle) and QI4 (bottom). The velocities vary from the horizontal (0^0) to vertical (90^0) direction of the wave normal. Left-hand plots correspond to $z = 0$ km, right-hand plots to $z = 1$ km.

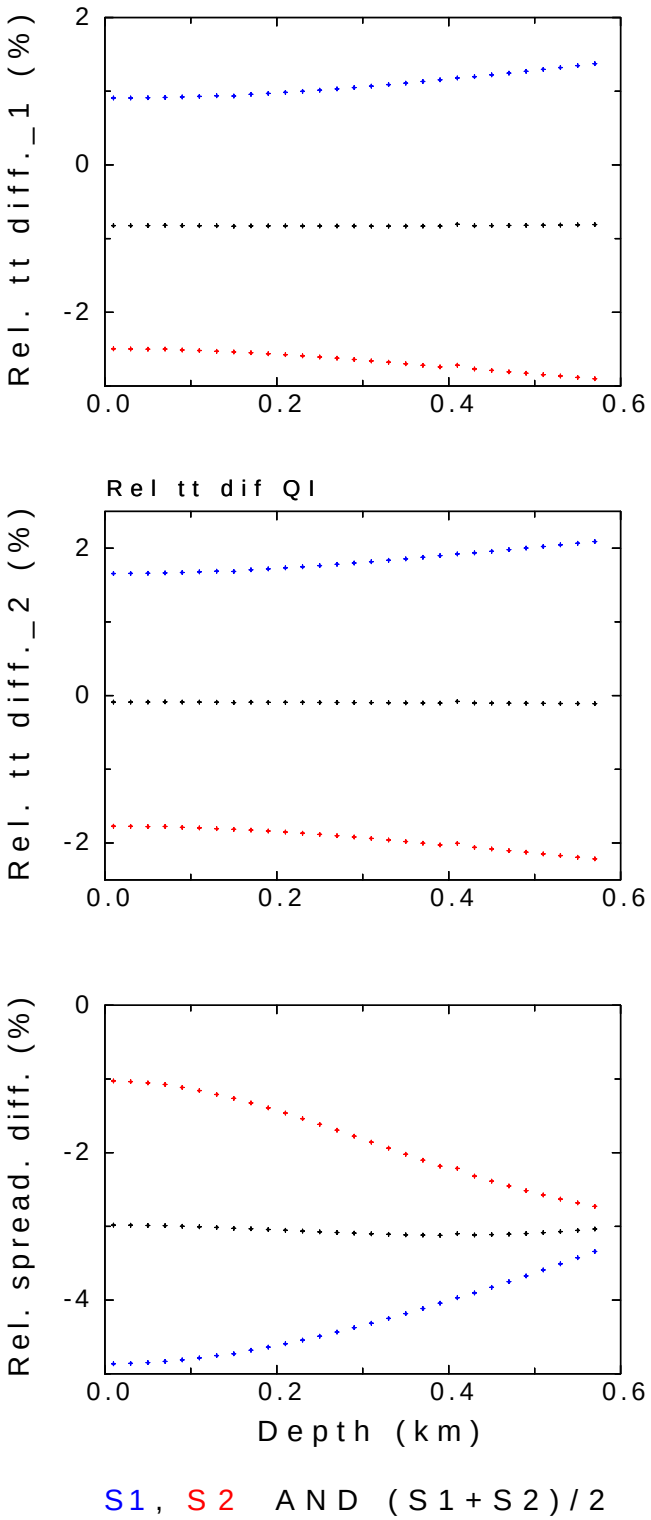

Figure 2: Model QI2 HOM. The relative first-order traveltime (top), the second-order traveltime (middle) and the geometrical spreading differences, see eq.(31), of quantities computed along the common S-wave ray and the exact quantities for the faster S1 (blue) and the slower S2 (red) waves and their averaged values (black).

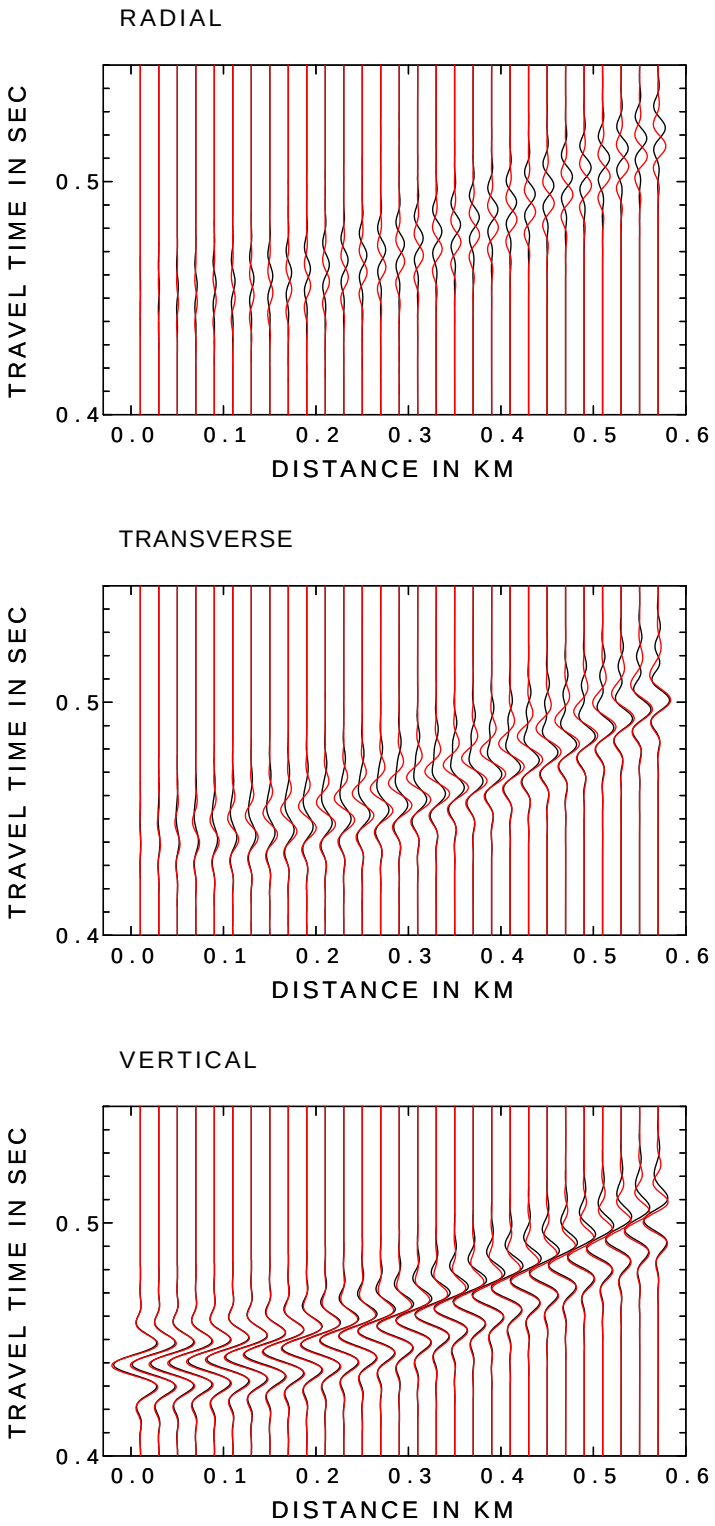

Figure 3: Comparison of the seismograms computed with the first-order coupling equations (19) (red) and the standard ray theory seismograms (black) for the vertical single-force source in the QI2 HOM model.

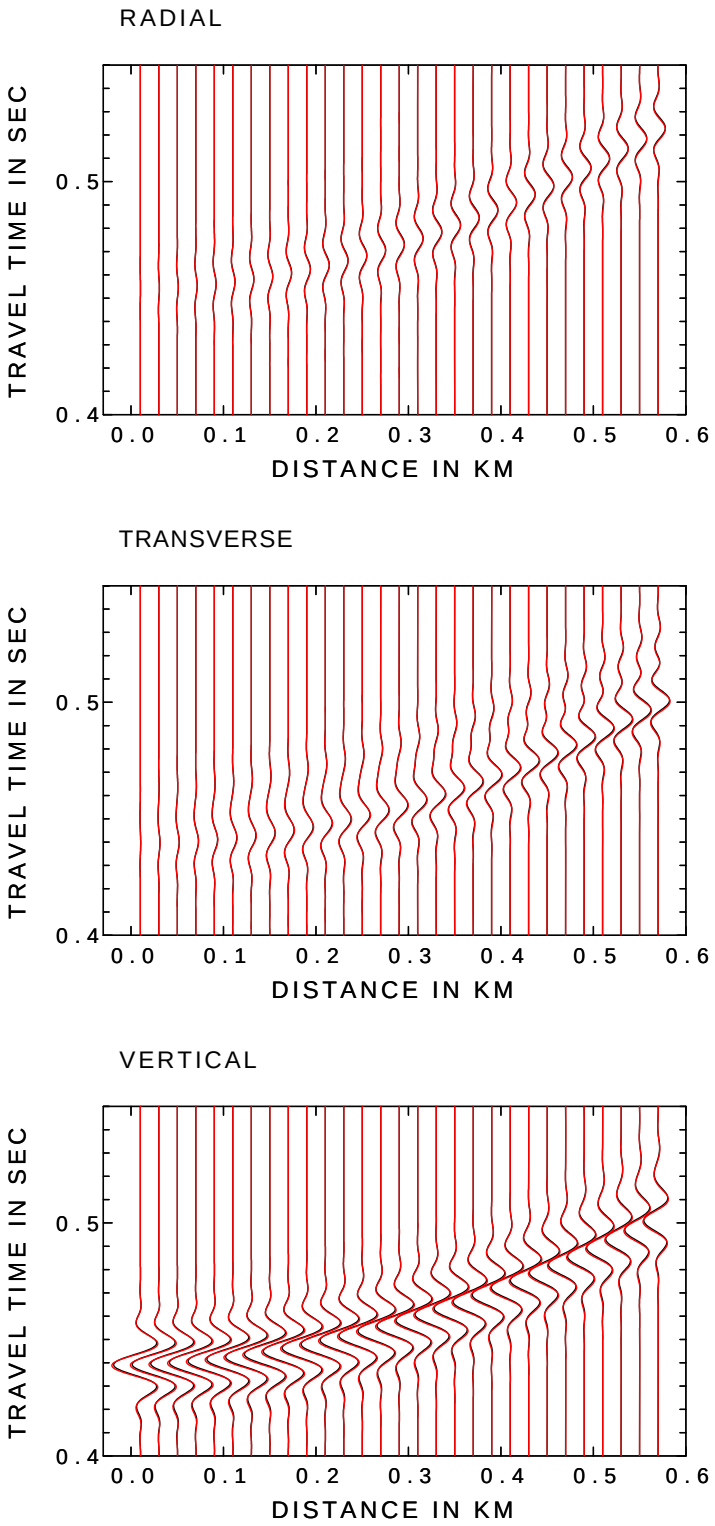

Figure 4: Comparison of the seismograms computed with the second-order coupling equations (29) (red) and the standard ray theory seismograms (black) for the vertical single-force source in the QI2 HOM model.

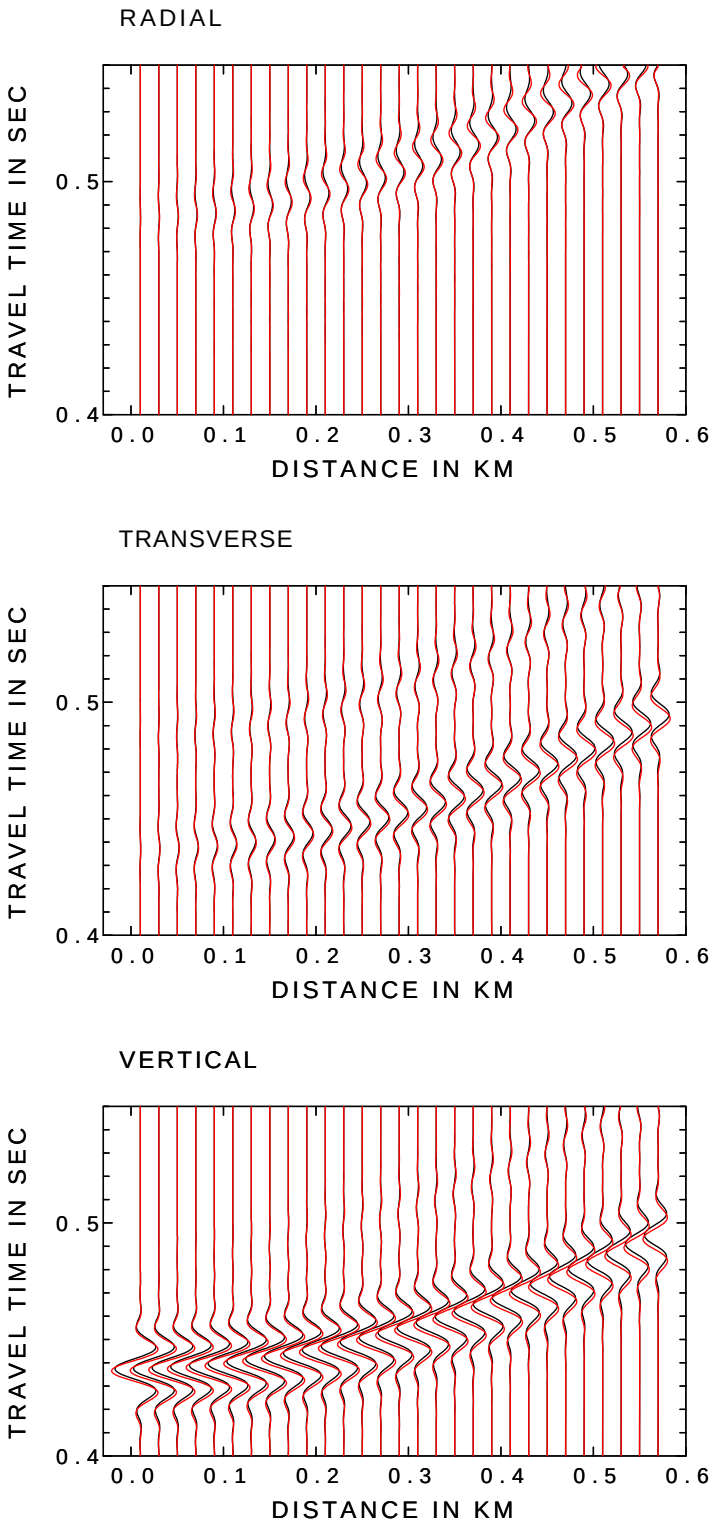

Figure 5: Comparison of the seismograms computed with the second-order coupling equations (29) (red) and the standard ray theory seismograms (black) for the vertical single-force source in the QI4 HOM model.

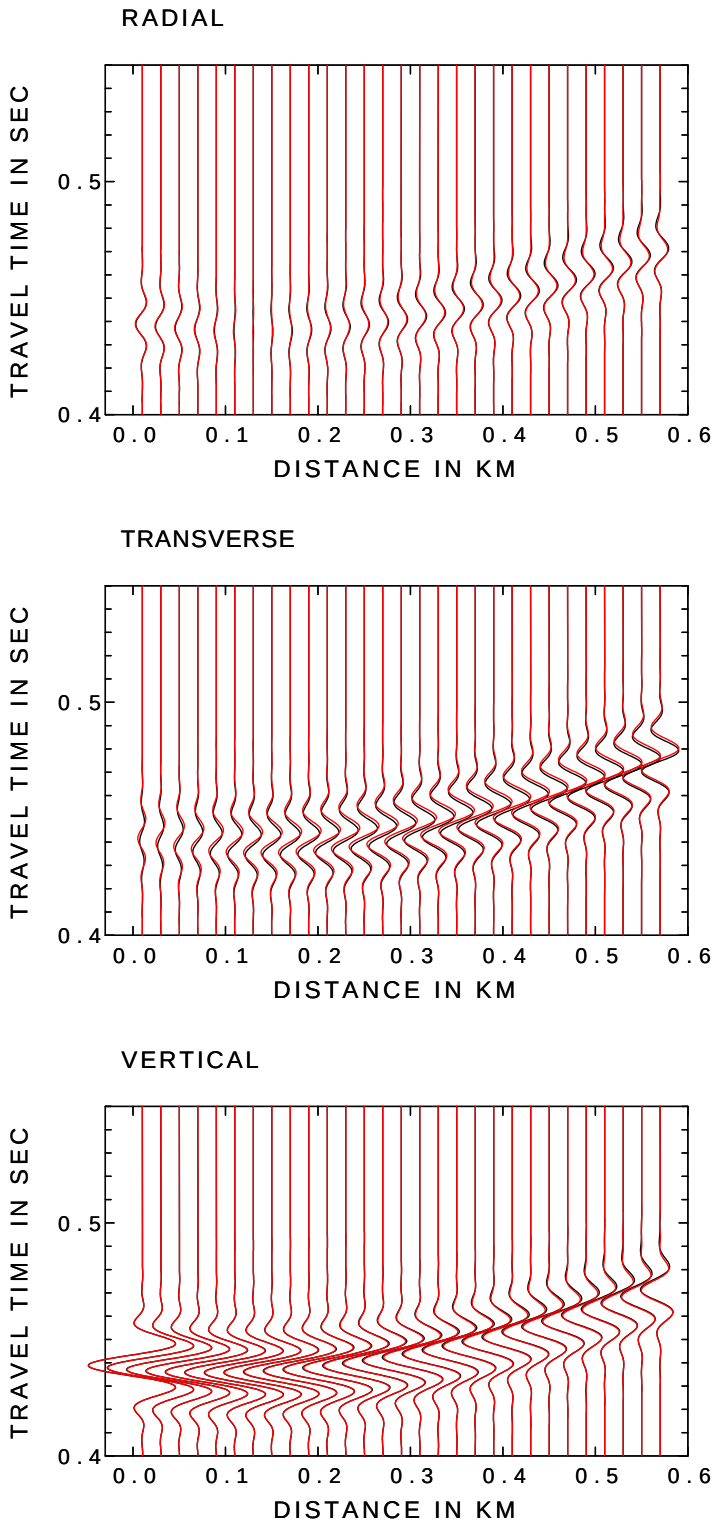

Figure 6: Comparison of the seismograms computed with the first-order coupling equations (19) (black) and the second-order coupling equations (29) (red) for the vertical single-force source in the QI model.

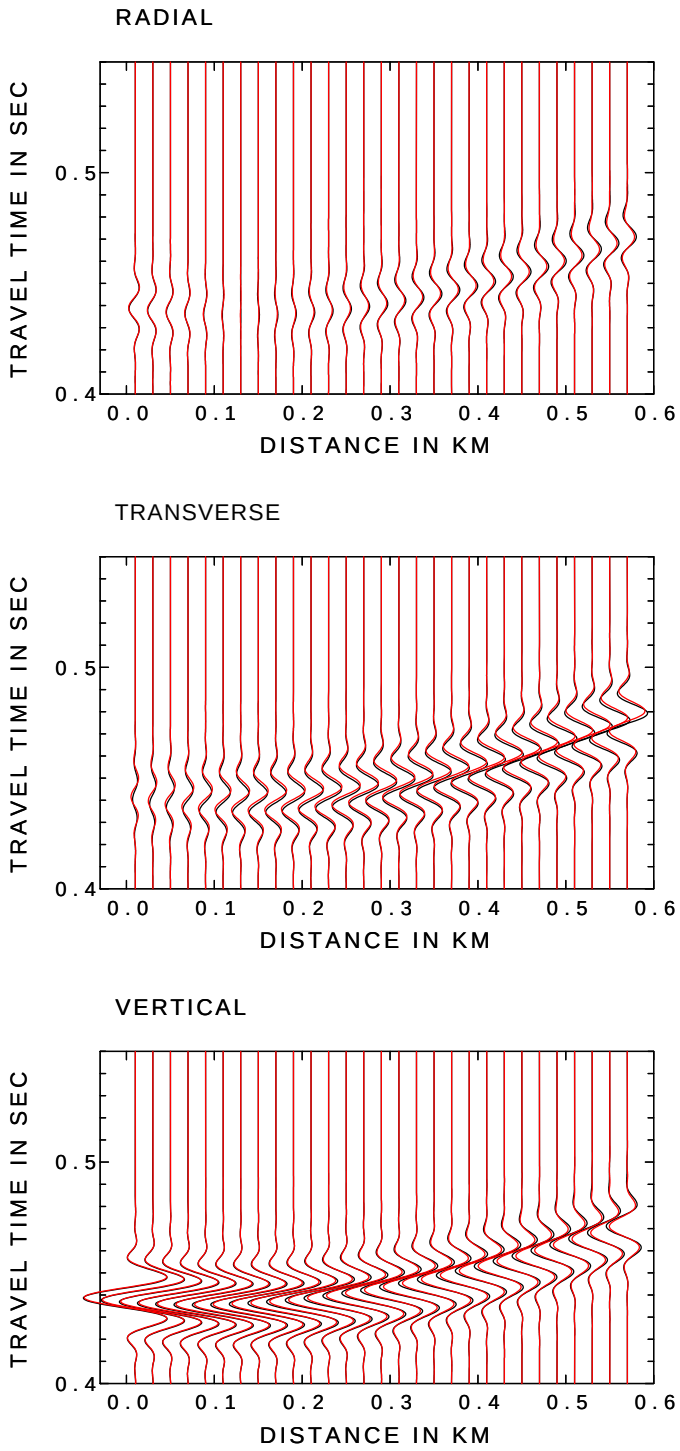

Figure 7: Comparison of the seismograms computed with the second-order coupling equations (29) (red) and the quasi-isotropic approach (black) for the vertical single-force source in the QI model.

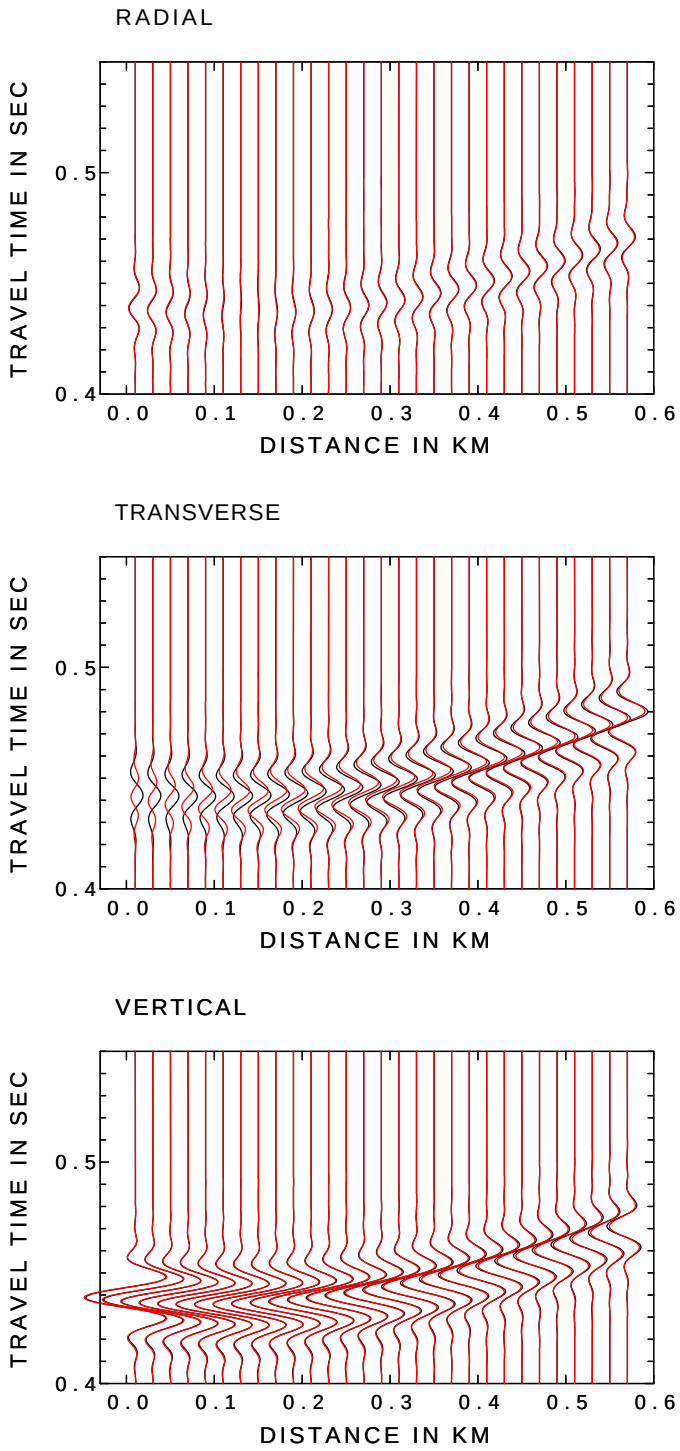

Figure 8: Comparison of the seismograms computed with the second-order coupling equations (29) (red) and the standard ray theory seismograms (black) for the vertical single-force source in the QI model.

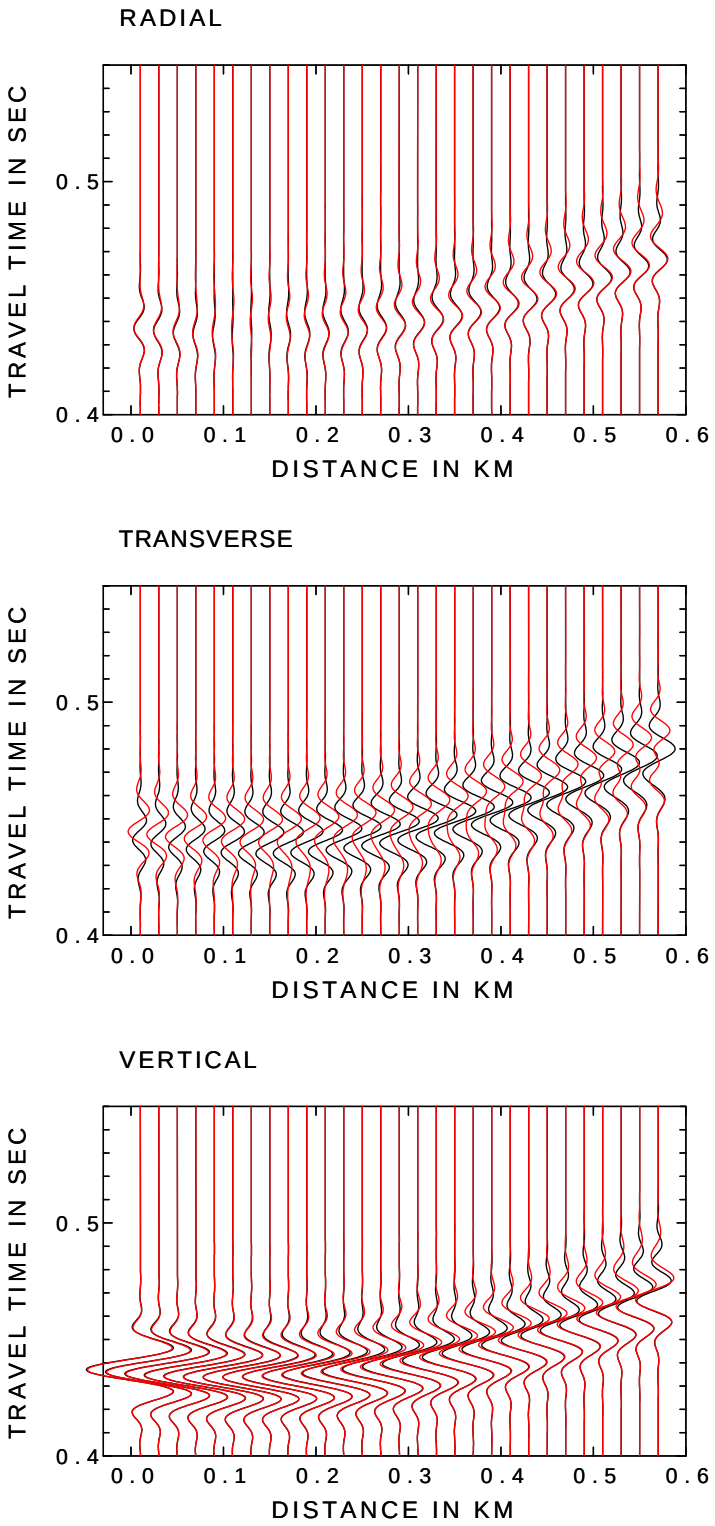

Figure 9: Comparison of the seismograms computed with the first-order coupling equations (19) (black) and the second-order coupling equations (29) (red) for the vertical single-force source in the QI2 model.

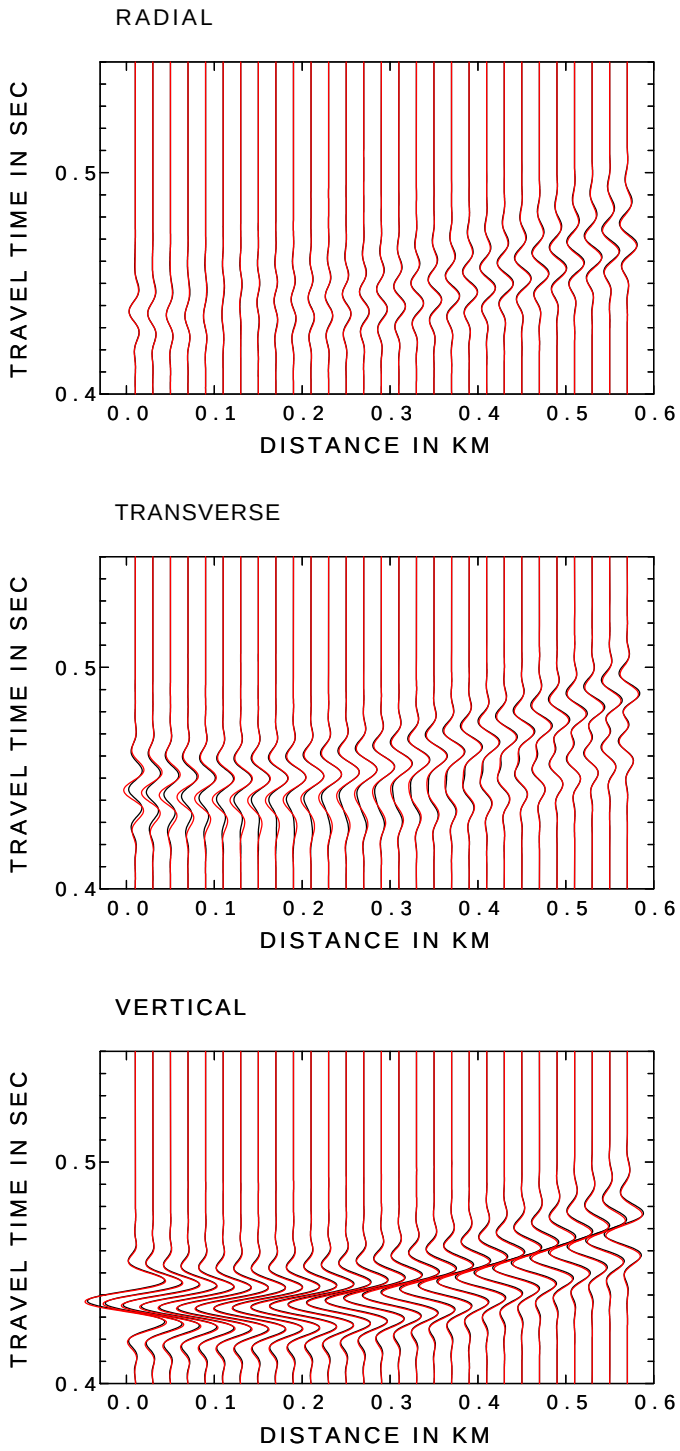

Figure 10: Comparison of the seismograms computed with the second-order coupling equations (29) (red) and the standard ray theory seismograms (black) for the vertical single-force source in the QI2 model.

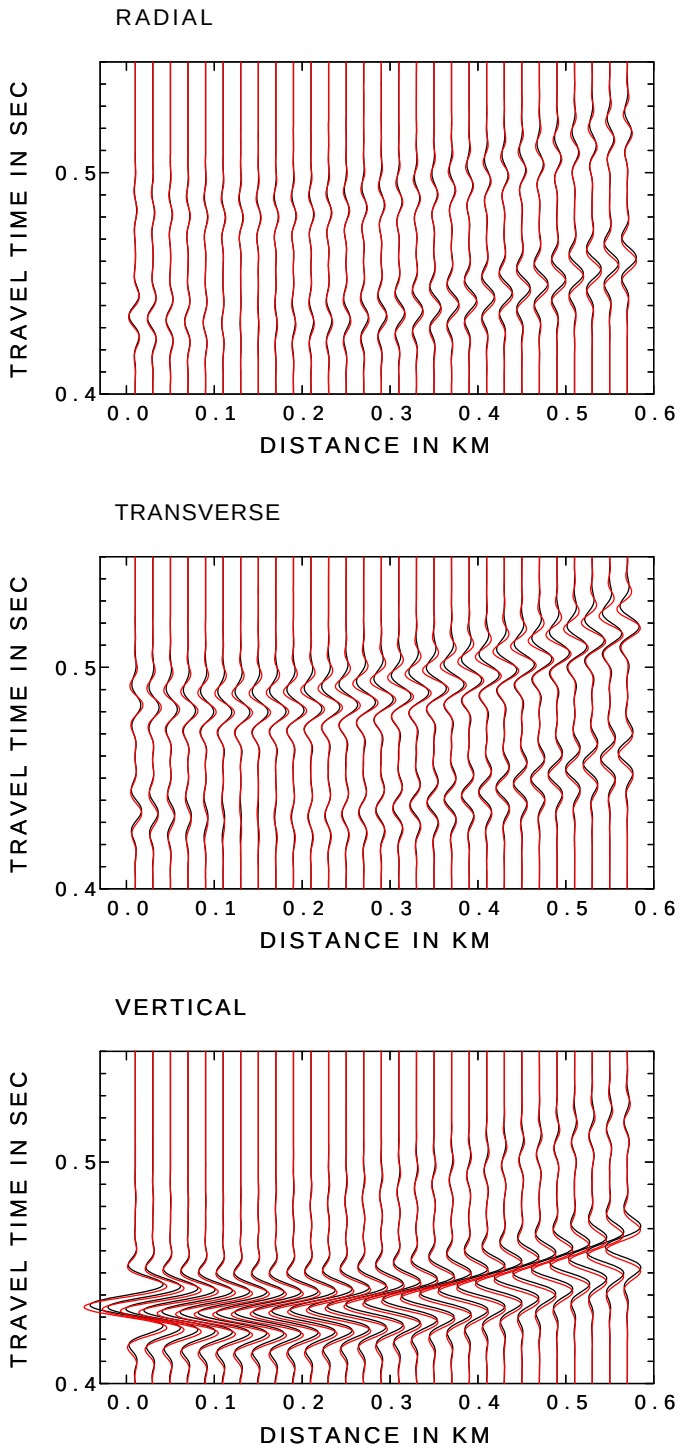

Figure 11: Comparison of the seismograms computed with the second-order coupling equations (29) (red) and the standard ray theory seismograms (black) for the vertical single-force source in the QI4 model.